Monthly Notices of the ROYAL ASTRONOMICAL SOCIETY

MNRAS **504,** 146–154 (2021) doi:10.1093/mnras/stab842
Advance Access publication 2021 March 30

Maximum black hole mass across cosmic time

Jorick S. Vink ,★ Erin R. Higgins, Andreas A. C. Sander and Gautham N. Sabhahit
Armagh Observatory and Planetarium, College Hill, Armagh BT61 9DG, UK

Accepted 2021 March 16. Received 2021 February 1; in original form 2020 December 30

ABSTRACT

At the end of its life, a very massive star is expected to collapse into a black hole (BH). The recent detection of an 85 $M_\odot$ BH from the gravitational wave event GW 190521 appears to present a fundamental problem as to how such heavy BHs exist above the approximately 50 $M_\odot$ pair-instability (PI) limit where stars are expected to be blown to pieces with no remnant left. Using MESA, we show that for stellar models with non-extreme assumptions, 90–100 $M_\odot$ stars at reduced metallicity ($Z/Z_\odot \leq 0.1$) can produce blue supergiant progenitors with core masses sufficiently small to remain below the fundamental PI limit, yet at the same time lose an amount of mass via stellar winds that is small enough to end up in the range of an 'impossible' 85 $M_\odot$ BH. The two key points are the proper consideration of core overshooting and stellar wind physics with an improved scaling of mass-loss with iron (Fe) contents characteristic for the host galaxy metallicity. Our modelling provides a robust scenario that not only doubles the maximum BH mass set by PI, but also allows us to probe the maximum stellar BH mass as a function of metallicity and cosmic time in a physically sound framework.

Key words: gravitational waves – stars: black holes – stars: evolution – stars: massive – stars: mass-loss – stars: winds, outflows.

1 INTRODUCTION

The direct detection of the first gravitational waves from the merger of two heavy black holes (BHs) in GW 150914 confirmed one of the toughest predictions of Einstein's theory of general relativity. But while satisfying the world of physics in general, for astrophysics this was only the beginning: many were surprised by the large BH masses of, respectively, 36 and 29 $M_\odot$ (Abbott et al. 2016), showcasing how the new field of multimessenger astrophysics had just re-opened the field of stellar evolution in a spectacular fashion. Stellar mass BHs had previously been revealed by their interaction in binary systems (Orosz et al. 2011), but the maximum stellar BH mass in our Milky Way is not higher than roughly 15–20 $M_\odot$ (Belczynski et al. 2010). While we know that very massive stars (VMS) above 100 $M_\odot$ exist (Crowther et al. 2010; Vink et al. 2015), this mass is significantly diminished via stellar winds already during core hydrogen (H) burning (Vink & Gräfener 2012). The heavy nature of the BH, as measured by LIGO/VIRGO therefore supported the assumption that the gravitational wave event occurred in a part of the Universe still pristine in its enrichment with heavy elements ('metallicity (Z)'), lowering stellar wind mass-loss (Vink, de Koter & Lamers 2001; Vink & de Koter 2005). A low-Z solution was widely accepted until the announcement of a 70 $M_\odot$ BH in LB-1 (Liu et al. 2019), spurring stellar evolution theorists to avoid heavy mass-loss in the Milky Way (Belczynski et al. 2020; Groh et al. 2020), either by arbitrarily lowering the mass-loss rates of VMS – seemingly contradicting VMS mass-loss calibrations (Vink & Gräfener 2012) – or by invoking the presence of a strong dipolar surface magnetic field that could quench the wind (Petit et al. 2017). While such magnetic fields in some 5–10 per cent of massive OB stars do indeed exist, no B-fields have yet been detected in VMS (Bagnulo et al. 2020). The problem of the formation of a 70 $M_\odot$ BH in a solar metallicity environment apparently resolved itself when the spectral signatures of LB-1 were re-interpreted (Abdul-Masih et al. 2020; El-Badry & Quataert 2020).

The recent discovery of GW 190521, involving the merger of a 85^{+21}_{-14} $M_\odot$ and a 66^{+17}_{-18} $M_\odot$ BH (Abbott et al. 2020), was not only record-breaking in terms of obtained BH masses, but also represents an exciting challenge. The masses of both BHs in GW 190521 are at the limit of what is called the second[1] mass gap between approx. 50–130 $M_\odot$, where stars cannot collapse into BHs due to pair instability (PI) resulting from electron–positron pair production (Fowler & Hoyle 1964).

Beside a regime where the whole star is disrupted by a so-called pair-instability supernova (PISN; Barkat, Rakavy & Sack 1967; Glatzel, Fricke & El Eid 1985; Fryer, Woosley & Heger 2001; Umeda & Nomoto 2002; Scannapieco et al. 2005; Langer et al. 2007; Kasen, Woosley & Heger 2011; Kozyreva et al. 2017; Mapelli et al. 2020), there is also a regime where electron–positron pair production does not disrupt the star as whole, but causes significant violent pulses leading to enhanced mass-loss before an eventual 'pulsational pair-instability supernova' (PPISN; Chatzopoulos & Wheeler 2012; Chen et al. 2014; Woosley 2017; Leung, Nomoto & Blinnikov 2019; Marchant et al. 2019). In contrast to PISNe, PPISNe are leading to a BH as there is a remaining iron core that collapses. Still, the pulses before the eventual collapse remove so much mass that the combination of PISNe and PPISNe leads to a significant 'forbidden' mass regime, where no first-generation heavy BH should be found. The lower boundary of this regime is commonly considered to be

★ E-mail: jsv@arm.ac.uk

[1]The first mass gap refers to a observational gap between the most massive neutron stars and 'lightest' BHs.

approximately 50 $M_\odot$ (Farmer et al. 2019; Woosley, Sukhbold & Janka 2020), as the hydrogen (H) envelope is generally assumed to be lost, either through binary interaction or through strong mass-loss in the most massive stars.

Given inherent uncertainties of both the BH masses and the second mass gap, it is mainly the 85 $M_\odot$ BH in GW 190521 that surprised the astronomical community and led to the speculation that such heavy BHs of up to 85 $M_\odot$ are most likely 'second-generation' BHs, implying they must have merged from lighter BHs in an earlier event (Abbott et al. 2020). The preferred solutions involve mergers of lower mass BHs or stars in dense cluster/galactic environments (Fragione, Loeb & Rasio 2020; Romero-Shaw et al. 2020), however, as *both* BHs in the system are above the 50 $M_\odot$ boundary, this would imply an arguably contrived situation involving at least two double mergers, i.e. at least involving four objects. While one cannot rule out such a scenario, we will show that the formation of heavy BHs of the order of 85 $M_\odot$ neither requires an earlier BH merger nor more exotic scenarios such as a modified gravitation theory (Moffat 2020). The aim of our paper is *not* to reproduce all aspects of GW 190521, but instead to critically assess core overshooting and mass-loss assumptions and to check if an 85 $M_\odot$ BH may be able to form under reasonable conditions. We will indeed reveal that our uncertain understanding of the evolution of (very) massive stars due to our limited knowledge of wind mass-loss has led to an underestimation of the lower boundary of the second mass gap at low metallicity (Z).

In the following, we will show that some blue supergiants (BSGs) at low, but not necessarily zero metallicity (Z), of the order of 90–100 $M_\odot$ can retain most of their H-rich envelopes and avoid the pair-instability (PI) regime. By critically assessing stellar wind mass-loss, we present a solution for what has been considered an 'impossible'[2] BH mass in a wide range of host environments.

2 EVOLUTION OF VERY MASSIVE STARS

In this paper, we show that BSGs of order of 90–100 $M_\odot$ can silently collapse to BHs. The prime reason this solution was not considered until the discovery of GW 190521 was that previous authors generally assumed the H-envelope to be lost, either due to binary Roche lobe overflow or strong mass-loss in an individual star, e.g. as a luminous blue variable (LBV). However, as the currently most robust estimates of close binarity in massive stars are of order of 50 per cent (Sana et al. 2013) and some of those will already merge on the H-burning main sequence, only a fraction of massive stars are expected to be subjected to Roche lobe overflow. Furthermore, while the most massive single stars may lose significant amounts of mass as LBVs at high Z, there is little evidence this would be the case at lower Z. In fact, the incidence of LBVs at low Z seems to suggest a drop in LBV phenomenology, on both empirical and theoretical grounds (Kalari et al. 2018; Vink 2018b; Grassitelli et al. 2020).

In short, there is no a priori reason to assume that VMS lose their H-envelopes, as was for instance the case in a recent extensive stellar evolutionary study (also with MESA) on PISNe and PPISNe, resulting in a lower boundary of the second mass gap of $\simeq$50 $M_\odot$ (Farmer et al. 2019). This particular study was based on model grids leading to high precision and small error bars. In fact it was even argued that mass-loss was one of the smaller uncertainties and that the $^{12}C(\alpha, \gamma)^{16}O$ nuclear reaction was the larger contributor to the error budget. However, as we will argue below, such small error bars may not be realistic if the assumption of the removal of the H-envelope is questionable. In our study, we do not aim for high precision, but we aim for accuracy, at least in the first instance, while precision studies are left for future works.

The aim of our paper is to show that VMS of order of 90–100 $M_\odot$ can lose little mass at low Z to still have a sufficient total mass reservoir available to produce a first-generation BH of order of 85 $M_\odot$. At the same time, the models need to avoid too large carbon–oxygen (CO) core masses, as otherwise pair production during oxygen (O) burning might produce pulses that could remove too much mass.

The most straightforward way to remain below this critical boundary is to start off with an initial mass ($M_{\rm init}$) that is comparatively low (of order of 90–100 $M_\odot$), as more massive stars have progressively larger convective cores (Yusof et al. 2013; Köhler et al. 2015; Vink et al. 2015). Furthermore, the fractional increase of the core by convective overshooting must remain relatively low in order to maintain a compact core, such as values found by Ekström et al. (2012) and Higgins & Vink (2020) of order $\alpha_{\rm ov} \simeq 0.1$. Note that we do *not* argue that *all* massive stars should necessarily have small cores, as there is plentiful evidence from astroseismology (Bowman 2020), eclipsing binaries (Higgins & Vink 2019), and the width of the main sequence (Vink et al. 2010; Brott et al. 2011) that many massive stars have larger cores, implying some form of extra mixing, commonly attributed to 'overshooting'. In this study, we show that small amounts of overshooting are needed to produce BSG progenitors that may retain a large fraction of their H envelope. Stars with larger amounts of overshooting would evolve to the red supergiant (RSG) phase where strong mass-loss would decrease the mass of the H-envelope. Astroseismology results in the mass range up to approx. 25 $M_\odot$ suggest overshooting values in terms of step overshooting $\alpha_{\rm ov}$ from values close to 0 up to 0.44 (Bowman 2020), with an equal if not slightly higher chance for low overshooting values of order $\alpha_{\rm ov} \simeq 0.1$ used for our BSG models than higher $\alpha_{\rm ov}$ cases. Given that what we are interested in here in our study is the *maximum* BH mass as a function of Z, we can be confident that this is set by the *low* overshooting, small core models, which we explore in the following.

3 MESA MODELLING

After describing our evolution strategy modelling, we utilize MESA (v12115; Paxton et al. 2011, 2013, 2015, 2018, 2019) and update its physics as described below. We evolve the objects at least through core O-burning and we check if the models encounter PI. Successful models for heavy BH formation thus require two key criteria. The first one is that of a CO core mass that remains below 37 $M_\odot$, the second criterion is that of a massive envelope (above about 40 $M_\odot$).

A representative set of models is listed in Table 1. The range of initial masses is comprised of 90–110 $M_\odot$ with initial metallicities of 1–10 per cent $Z_\odot$. The initial composition of each model encompasses a scaled-solar metallicity based on the abundances by Grevesse & Sauval (1998) with $Y = 0.266$ and $Z_\odot = 0.017$. This scaling is also applied to the employed OPAL opacity tables from Rogers & Nayfonov (2002).

The standard mixing length theory of convection by Böhm-Vitense (1958) is included with $\alpha_{\rm MLT} = 1.82$ (Choi et al. 2016). The Ledoux criterion is employed with standard semiconvective mixing described by an efficiency parameter $\alpha_{\rm sc} = 1$. We incorporate extra mixing by convective core overshooting via the 'exponential-overshooting' method. This overshooting description assumes an

[2]We place the word 'impossible' between inverted commas as there is no fundamental physical limit being broken.

Table 1. Fundamental parameters of our representative models, including the initial metallicity Z and mass $M_{\rm init}$. For all models, we also list the total mass $M_{\rm f}$, envelope mass $M_{\rm env}$, and CO core mass $M_{\rm CO}$ of the final model stage. Models that are subject to PI were stopped at this point.

Model	$Z/Z_\odot$	$M_{\rm init}$	$M_{\rm f}$	$M_{\rm env}$	$M_{\rm He}$	$M_{\rm CO}$	
A1	0.1	90	80.4	42.9	37.5	32.7	cc
A1-Alt	0.1	90	74.0	35.2	38.8	33.8	cc
A2	0.1	110	–	–	45.1	39.5	PI
B1	0.01	90	87.0	46.1	40.9	34.6	cc
B2	0.01	110	–	–	52.8	45.6	PI

exponential mixing profile that decays as a function of distance from the core. The extent of this mixing region is defined by the parameter $f_{\rm ov}$ that gives a measure of inverse of the slope of the exponential decay. The diffusion coefficient in our models decreases from D_0 near the core ($f_0 = 0.001$ times the pressure scale height below the core) until a minimum coefficient of $D_{\rm min} = 0.01$ is reached. Overshooting dredges extra H from the envelope into the core during H-burning, meaning that the helium core will be larger with increased $f_{\rm ov}$. In our models, we use $f_{\rm ov} = 0.01$ (equivalent to step-overshooting $\alpha_{\rm ov} = 0.1$). While this treatment is common in the evolution models of massive stars (Ekström et al. 2012; Higgins & Vink 2020), it is a crucial parameter deciding stars become blue or red supergiants. According to recent calculations (Farmer et al. 2019), a CO core above $\sim 37\,{\rm M}_\odot$ (corresponding to an He core of $\sim 50\,{\rm M}_\odot$) would lead to PI. Our models yielding massive BHs have CO core masses below this limit (cf. Table 1), but could enter this regime for considerably larger efficiencies of overshooting.

The MLT^{++} routine in MESA has been used to evolve stars with very high initial masses through their post-main-sequence stages by reducing the superadiabaticity in the radiatively dominated envelopes. Our models use the standard MLT^{++} values set in MESA. MLT^{++} essentially reduces the contribution of radiative energy transport and offers an alternative, more efficient energy transport mechanism in these regions. MLT^{++} is activated in all regions where the superadiabaticity is greater than $f_1 = 10^{-4}$, irrespective of the fraction of energy transported by radiation ($\lambda_1 = -1$). The actual reduction in superadiabaticity is determined by the parameter $f_2 = 10^{-2}$, with smaller values resulting in larger reduction in superadiabaticity. Although MLT^{++} has a physical significance, its usage here is a numerical necessity for such high-mass models to evolve to late burning stages without technical problems, e.g. due to extremely short time-steps (Paxton et al. 2013).

The effects of rotation have been included with the transport of angular momentum and chemical elements treated as diffusive processes through rotationally induced instabilities. These instabilities include dynamical and secular shear instabilities as well as the Solberg–Høiland, and Goldreich–Schubert–Fricke instabilities, and Eddington–Sweet circulation. The effects of a Spruit–Taylor dynamo have not been included in our models, allowing for differential rotation rather than solid-body rotation. The efficiencies of these instabilities are included as described by Heger, Langer & Woosley (2000). For all models, we implement a rotation rate as a function of the critical velocity for each mass with $\Omega/\Omega_{\rm crit} = 0.2$, corresponding to rotation rates of $\sim$150 km s^{-1}. Since the effects of rotation lead to larger core sizes with increased $v_{\rm rot}$, a slower rotation is preferred to keep the core compact and reach the maximum BH mass. Faster rotating stars will likely form lower mass BHs as the increased rotation will not only increase the core size, but beyond a certain limit also promote bluewards evolution towards a Wolf–Rayet (WR) star, which will lose a significant portion of the total mass by the time of core collapse.

All models are calculated with the 'standard' time-step resolution of 10^{-4} and are evolved until core collapse unless convergence issues occur at earlier stages. In all cases, our models have been evolved to core O-burning, where models either reach the PI criteria or continue O-burning until a BH is formed. In MESA, models that undergo pulsations at the onset of core O exhaustion due to pair production prompt a condition when γ – summed over all cells – falls below 4/3. MESA models of massive stars undergoing pulsational PI during O burning have been previously studied in Farmer et al. (2019), although in the context of pure helium stars. The presence of a massive envelope in our models ($>35{\rm M}_\odot$) during O burning (e.g. in our model A1) helps to avoid this $\gamma < 4/3$ regime.

Fig. 1 showcases the stellar structure of our model A1 (a $90\,{\rm M}_\odot$ star at 0.1 $Z_\odot$) as a function of evolutionary time-scale ('Kippenhahn diagram'). For the purpose of calculating our stellar models within the scope of this study, we have adopted the standard treatments of convection and rotation in stellar evolution, as well as the common sets for atomic data and nuclear reactions. While we have assessed the parameter space around our adopted inputs, we find that our conclusions are not impacted by the implementation of convection parameters or the necessary treatment of the technical aspects, such as the use of MLT^{++} to run stellar models with high initial masses to late evolutionary stages.

In contrast, choices that affect the physics determining the eventual CO core size and the loss of envelope mass are very important for our results. Therefore, we have tested the extent of core overshooting during core H-burning, rotation rates, and the implementation of mass-loss through stellar winds. We find a strong dependence on the amount of overshooting, such that a small fractional increase is preferable to maintain a compact core. Similarly, a modest rotation rate is required to keep the core compact and avoid evolution towards homogeneously mixed stars. Consequently, we estimate that our scenarios for forming massive BHs just below the PI limit are applicable for stars with initial surface rotation velocities of ~50–200kms^{-1}, which is representative for the bulk of observed massive stars at low metallicity (Ramírez-Agudelo et al. 2013).

4 IMPROVED TREATMENT OF WIND MASS-LOSS

As stellar mass is the prime quantity for stellar evolution, the loss of mass due to stellar winds is a decisive factor in massive star evolution. The rate of mass-loss is a complex function of stellar properties such as the stellar effective temperature that changes during the evolutionary track. Therefore, evolution models rely on physical, theoretical, or empirical descriptions for specific temperature ($T_{\rm eff}$) regimes. The application of such formulae beyond the validity regime where they were established has to be carefully considered, as inadequate extrapolations may lead to over- or underestimations by orders of magnitude (Sander & Vink 2020).

A standard approach inherent to state-of-the-art stellar evolution codes is the collection of various mass-loss treatments. In MESA, the generally applied formula for massive stars is the so-called Dutch wind scheme. For hot stars on the main sequence, the models rely on line-driven Monte Carlo radiative transfer calculations (Vink et al. 2001), while a different relation involving dust driving is employed for cooler star winds (de Jager, Nieuwenhuijzen & van der Hucht 1988). For stars that have their outer H envelope removed, a third formula for Helium stars is employed. In MESA and other state-of-art codes, this final formalization is generally based on an empirical

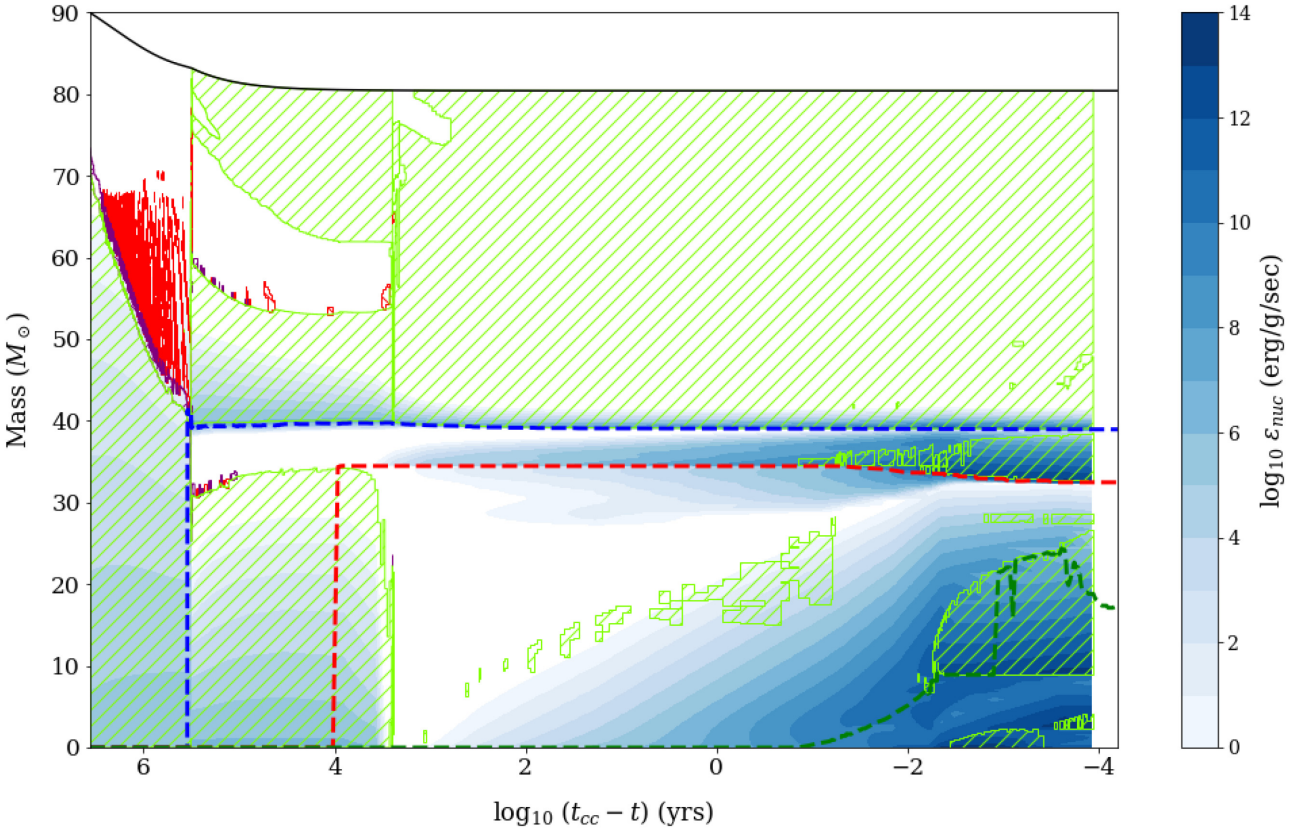

Figure 1. Evolution of the internal structure of our model A1 with initial mass 90 $M_\odot$ and metallicity 0.1 $Z_\odot$, as a function of mass ($M_\odot$) and time until core collapse. The colour bar represents the nuclear burning regions. The green hatched region denotes the convective zones, purple region denotes the small overshooting layer above the H-burning core, and the red region denotes layers with semiconvective mixing. The dashed blue and red lines represent the He and CO core boundaries, respectively.

study of WR stars in the Milky Way (Nugis & Lamers 2000). This final treatment does not accurately reflect the wind physics at the low metallicities considered in the context of massive BHs as GW progenitors.

In our stellar evolution models discussed below, those that include our improved wind treatment, such as A1 and B1, are able to maintain their H envelopes intact. Those with the standard MESA treatment, such as model A1-Alt, lose extra mass when the model switches either to the RSG recipe (as is the case for A1-Alt) or to the WR recipe as was the case for some other test models. Either way, in this MESA 'Dutch' standard treatment, there is rapid envelope loss during core He-burning, even at low Z.

The reason for the strong mass-loss in model A1-alt is the early switch from a hot star wind treatment (Vink et al. 2001) to the one for cool stars (de Jager et al. 1988). The mass-loss description for the cool star regime is employed to describe dusty RSGs, which have temperatures of just 3000–4000 K. While the switch in the standard treatment occurs already at 10 000 K, the BSGs in this temperature range (8000–12 000 K) are too hot to form dust and their winds are expected to be driven by iron-dominated gas opacities rather than dust. Consequentially, the utilization of the treatment of dust-driven winds leads to an overestimation of the actual mass-loss, and our modelling would not be able to make BHs more massive than 75 $M_\odot$.

When we employ the more physical line-driven wind description in this regime for stars above the so-called second bistability jump above 8000 K (Petrov, Vink & Gräfener 2016), all our model stars are BSGs, avoiding the regime of the RSGs, and can retain a sufficiently large amount of their H envelope to make BHs of order of 80–87 $M_\odot$ at low Z (see models A1 and B1).

As was already alluded to, another aspect inherent to evolution modelling with codes such as MESA is the employment of the third formula. Intended to describe the mass-loss of He-enriched WR stars (Nugis & Lamers 2000), it is applied to evolved stars above 10 000 K. As the mass-loss scales with iron content, but not with metals that can be produced via self-enrichment such as CNO (Vink & de Koter 2005; Sander, Vink & Hamann 2020), we apply the physically motivated standard hot star wind treatment (Vink et al. 2001) also for our evolved models as a WR-like treatment would yet again lead to artificially high mass-loss rates at low Z.

4.1 Potential extra mass-loss near the Eddington limit

A potential concern for the proposed heavy BH scenario would occur if the suggested wind treatment would underestimate mass-loss rates in close proximity to the Eddington limit (Vink et al. 2011) or even above the Eddington limit due to continuum driving (Shaviv 2000). The first question concerns mass-loss during core H burning as this is where the stars spend most of their lifetime. Electron scattering values during core H burning for model A1 are only of the order of 0.3 which ensures that the metallicity-dependent rates of Vink et al. (2001) are safely applicable. The next potential hurdle could occur during the approximately 10 times shorter core He burning phase. In this phase, the electron scattering Eddington parameter climbs to 0.7, which is marginally larger than the values that were employed for the derivation of the (Vink et al. 2001) parametrization, but checking

more recent Monte Carlo computations by Vink (2018a) show that the mass-loss rates stay comfortably low (of order of 10^{-5} $M_\odot$ yr^{-1}). At very low Z additional metal line opacities would not change this assertion, but for our case we tested the 'worst case' scenario of the total Eddington value for model A1 at 10 per cent the solar metallicity using the sophisticated 1D POWR stellar atmosphere code (Gräfener, Koesterke & Hamann 2002; Sander et al. 2020), which provides the most accurate (flux-mean) opacities in 1D.

From the analysis of the POWR atmosphere models, we conclude that while the metallicity-dependent continuum opacity is larger than that of just electron scattering, the values remain sub-Eddington, and a continuum driven wind is not launched during core-He burning. Metallicity-dependent line driving needs to be carefully analysed in order to assess if the predicted mass-loss rates from Vink et al. (2001) are significantly underestimated in this regime. If mass-loss rates are as high as 10^{-4} $M_\odot$ yr^{-1}, of order 10 solar masses could potentially be lost during core He burning. However, mass-loss rate predictions in this regime are highly uncertain and still in its infancy, and it would be equally or more likely that the true mass-loss rates are lower than 10^{-4} $M_\odot$ yr^{-1} in which case a negligible amount of mass would be lost during core He burning. As the key physics involve metallicity-dependent driving, even in the worst case scenario of a high mass-loss rate, our proposed scenario would still be valid, but merely the critical metallicity, where we have a steep drop in the maximum BH mass, would shift towards lower Z by approximately a factor of two.

Note that in reality, atmospheres in close proximity to the Eddington limit might either inflate (Gräfener, Owocki & Vink 2012) or become porous (Shaviv 2000). In such cases, 3D hydrodynamical modelling (Jiang et al. 2018) would become necessary. Future 3D radiative driving and hydrodymical stellar models (Grassitelli et al. 2020) are needed for accurate physical modelling, as current 3D hydrodynamical models still rely on approximate Rosseland mean opacities.

While our detailed atmosphere models show that we do not reach a regime of continuum-driven winds during core-He burning, this could happen in the very last stages of evolution. Here, the excess luminosity is so high that super-Eddington mass-loss is likely. However, the time-scales for this mass-loss are low, thus leading to modest time-averaged mass-loss rates. For numerical reasons, it is a standard procedure in stellar evolution modelling to not include explicit mass-loss during late burning stages. However, we can do a common posterior estimation (Renzo et al. 2020) by assuming that all the luminosity that exceeds the Eddington limit can be used to remove mass that leaves the star with a velocity similar to the escape speed. Integrated over the whole time after core-He burning, this leads to a loss of 0.19 $M_\odot$. This value is comparable to the amount of mass lost during core collapse and negligible in the context of our overall scenario.

5 RESULTS

Model A1, a 90 $M_\odot$ star at 0.1 $Z_\odot$, becomes a BSG around 10 000 K (see the HRD of Fig. 2) and eventually collapses into a BH of 80 $M_\odot$. Note that this model evolves through all stages up to Si burning with a final CO core mass of 32.7 $M_\odot$. At this point, the star retains a massive, H-rich envelope of 42.9 $M_\odot$, which is even larger than the CO core. Contrary to common visualizations of evolutionary tracks of VMSs where phases beyond core He-burning are usually omitted, we do show the full evolution in Fig. 2, including the shorter O-burning phase where the HRD positions are less certain (e.g. Belczynski et al. 2020; Renzo et al. 2020).

In contrast to recent calculations determining the maximum BH mass below the PI gap (Farmer et al. 2019; Woosley et al. 2020), we do not a priori assume that stars forming heavy BHs must have lost their outer envelope. Instead, we have critically assessed the treatment of mass-loss for different temperatures employed in massive star evolution codes and improved their physical treatment, scaling the mass-loss rate with iron (Fe) which is the host galaxy metallicity.

Generally for massive stars below the Humphreys–Davidson limit, stellar evolution models encounter significant mass-loss during the helium (He) burning phase as cooler RSGs. To simulate this, we also evolved a star with the same properties as model A1 but now employing the standard mass-loss treatment with higher rates. This model (A1-Alt) dips into the RSG regime where its mass-loss rate increases by more than an order of magnitude. This leads to higher mass-loss during He burning, and although the model collapses to a BH, its final mass is never found to be above 75 $M_\odot$. For higher mass initial masses (e.g. 110 $M_\odot$, Model A2), the resulting BH mass does not grow either as the resulting PI would either remove the mass in pulsations or destroy the star completely. We do not follow these pulsations as this is not the focus of our study, but stop our calculations entering the PI regime.

5.1 The role of metallicity

As a next step, we explore the maximum BH mass across cosmic time by assessing the role of initial host Z. Models B1 and B2 have one order of magnitude lower Z than models A1 and A2. Model B1 with an initial 90 $M_\odot$ now forms an 87 $M_\odot$ BH, while the 110 $M_\odot$ model B2 still reaches the PI regime due to its higher CO core. Our metallicity exploration thus tells us robustly that the resulting maximum BH mass is approximately 90–100 $M_\odot$, which is in line with the masses inferred for all currently known GW events, including GW 190521, as well as marginal triggers, which are GW candidates with signal-to-noise ratios just below the standard threshold for detection (Udall et al. 2020).

As mentioned earlier, we do not claim that *all* 90–100 $M_\odot$ stars at low Z produce such heavy BHs. Statistics from GW events seem to indicate a break in the BH mass distribution around 40 $M_\odot$ (Fishbach & Holz 2020; The LIGO Scientific Collaboration & the Virgo Collaboration 2020) and The LIGO Scientific Collaboration & the Virgo Collaboration (2020) find that only ∼3 per cent of systems have primary masses greater than 45 $M_\odot$. This is partly expected to be a result of the Z-dependent upper BH mass that we infer in this paper, but we also wish to remind the reader that even independent of the Z argument, some massive stars will interact with a binary companion, and as also discussed earlier there is evidence for higher values of core-overshooting for several massive stars. In other words, our low-Z 'small core' solution for an 85 $M_\odot$ BH only covers a part of the parameter space (at the maximum), and further parameter studies are needed for inferences on BH populations.

A summarizing sketch of our findings is given in Fig. 3. The darkest blue shaded area shows the range of BH masses as a function of Z. The blue line represents the maximum BH mass. For low-Z stars, the limit is set by PI where BHs cannot exist (illustrated by the grey region). At a threshold metallicity, the maximum BH mass steeply declines due to the removal of the envelope by Z-dependent winds. At high Z, the maximum BH mass drops below the limit set by PI, but is now set by the further removal of layers via Z-dependent wind mass-loss.

The red solid line outlines the previous PI limit of order of 50 $M_\odot$ set by the maximum CO core mass (of ∼ 37 $M_\odot$) along with a

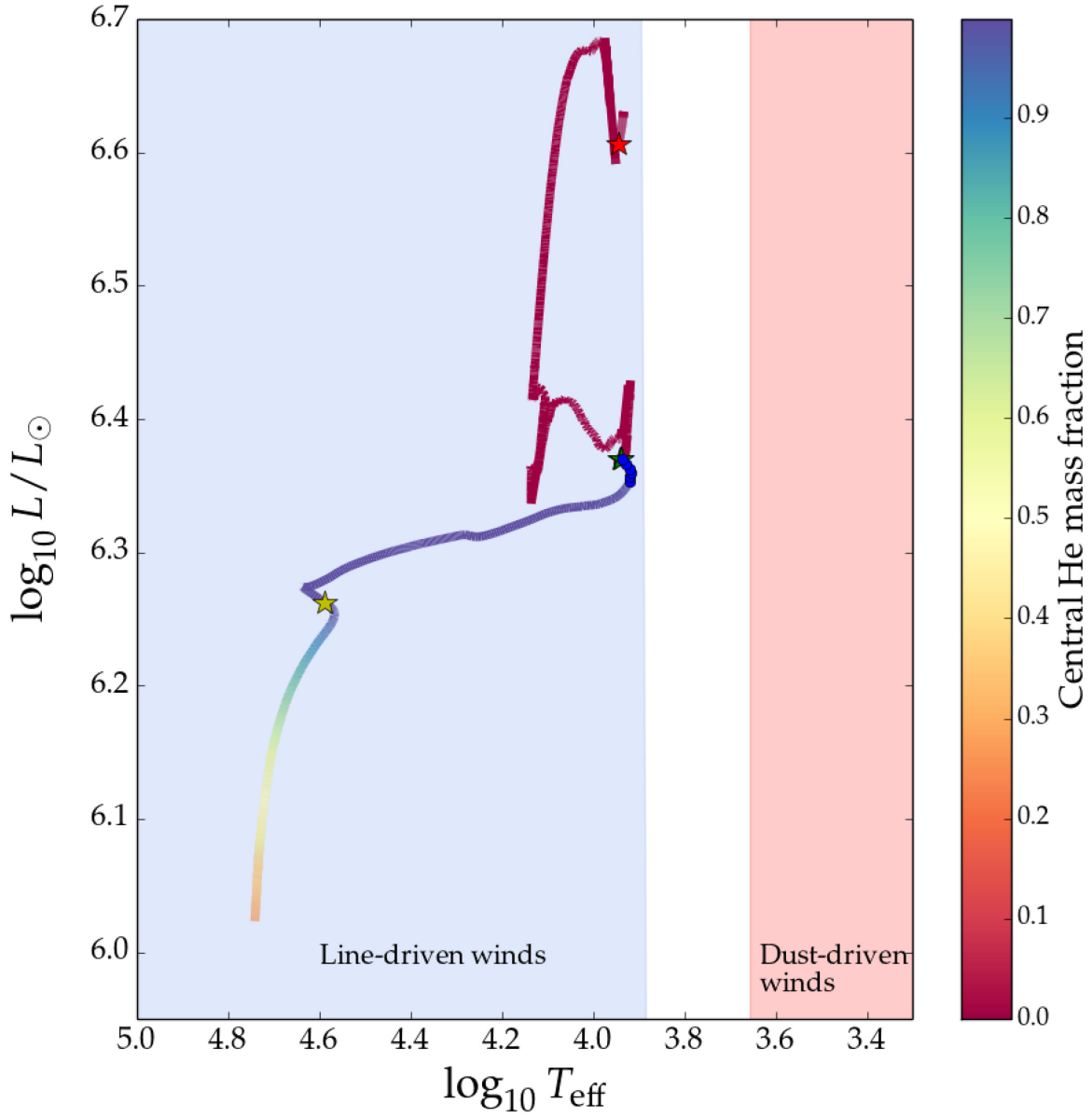

Figure 2. Evolution of model A1 in a Hertzsprung–Russell diagram. The colour bar represents the core He abundance, with a yellow star showing the TAMS position, a blue star illustrating the end of core He-burning, and a red star marking the end of core O-burning. Blue dots (near the blue star) show time-steps of 50 000 yr after core H exhaustion, where time is spent as a BSG (i.e. above log $T_{\rm eff} > 3.65$). Shaded regions highlight the area in the HRD where RSGs (red) evolve with dust-driven winds or BSGs (blue) evolve with line-driven winds.

diminished envelope. As we illustrate in Fig. 3, the infall of the envelope allows the BH to effectively *double* the previously obtained mass limits (Woosley 2017; Farmer et al. 2019) which were based on absent or significantly decreased envelopes. A pivotal outcome of our study is that the maximum *initial* mass to avoid pulsations does not significantly change with metallicity below a certain threshold Z, compared to the amount of retained envelope mass that changes drastically with metallicity.

5.2 The silent collapse of the star

To actually identify the final masses of our evolutionary models with the resulting BH masses, the core collapse of the star should not be accompanied by a supernova explosion as this might lead to a considerable loss of mass. Indeed, massive stars below the (pulsational) PI regime are most likely to produce an immediate BH – a so-called failed supernova – if their core is compact enough (O'Connor & Ott 2011; Ertl et al. 2016).[3] This is fulfilled for all of our models avoiding PI (A1, A1-Alt, B1). Still, to reach the high BH masses observed in recent GW events, also the outer layers of the star need to fall into the newly formed BH. To avoid a significant ejection of mass from the outer layers at core collapse, thus also the envelope needs to be sufficiently compact.

[3]See also Gilkis, Soker & Papish (2016) and Burrows et al. (2020) for alternatives to 'failed' supernovae and compactness respectively. For cases where rotation induces more mass-loss in the collapsar, see also Zhang, Woosley & Heger (2008), Nagataki et al. (2007), Tominaga (2009), and Woosley & Heger (2012).

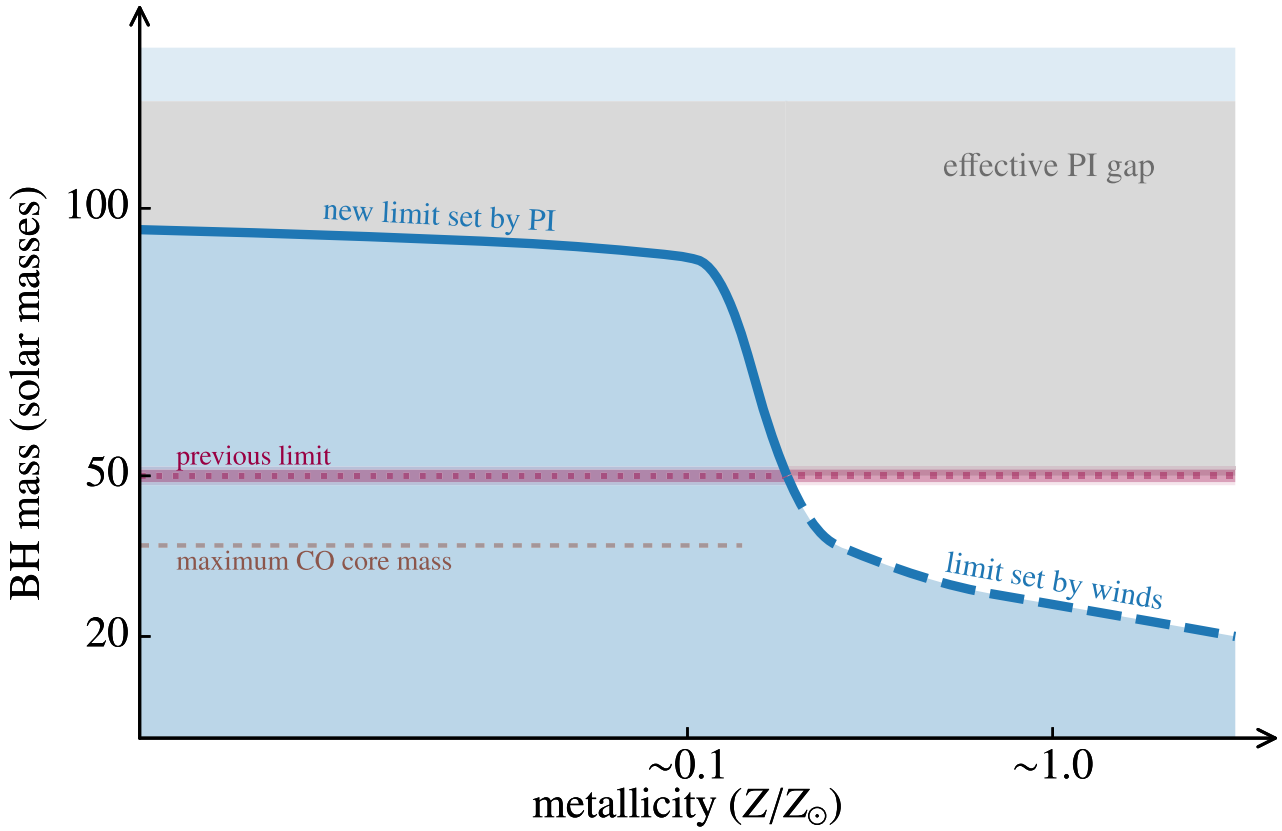

Figure 3. Schematic view of the maximum BH mass below the PI gap as a function of metallicity: at low Z, the maximum BH mass (blue solid line) is set by PI, where above this line the PI gap (grey region) is shown. Above a threshold metallicity, the maximum BH mass is determined by Z-dependent stellar winds (blue dashed line). The red line sets the previous maximum BH mass below the PI gap, while the light blue region at the top of the diagram provides the upper limit of the PI gap.

To determine whether our stars modelled in the evolutionary calculations undergo a silent collapse including also the envelope, we study the so-called compactness of the core and the envelope. A common measurement for the core compactness (O'Connor & Ott 2011; Ertl et al. 2016) is the parameter

$$\xi_{2.5} = \frac{2.5}{r(M = 2.5\mathrm{M}_\odot)[1000\,\mathrm{km}]}. \quad (1)$$

Our models at 0.1 $Z_\odot$ avoiding PI have a core compactness of $\xi_{2.5} = 0.77$ (models A1 and A1-Alt). While the lower boundary of $\xi_{2.5}$ for a failed supernova is still a matter of debate (Ertl et al. 2016), this value is considerably above all estimates for what is considered to be able to explode as a supernova (Ertl et al. 2020). Moreover, with CO core masses of over 30 $\mathrm{M}_\odot$, all of our models remaining below the PI gap are in a regime where recent studies expect them implode directly at the end of their life (Ertl et al. 2020; Woosley et al. 2020) until Fe core due to time-step problems.

To check, what fraction of the envelope falls into the newly formed BH, we consider the envelope compactness parameter (Fernández et al. 2018)

$$\xi_{\mathrm{env}} = \frac{M_\mathrm{f}[\mathrm{M}_\odot]}{R_\mathrm{f}[\mathrm{M}_\odot]} \quad (2)$$

with M_f and R_f denoting the total mass and radius of the star at core collapse. At the time of core collapse, our model stars will appear as BSGs with $\xi_{\mathrm{env}} = 0.1$. While not as compact as WR stars, this is an order of magnitude higher than for RSGs, meaning that the amount of ejected mass is fairly low. Based on recent simulations for ejecta masses in failed supernovae (Fernández et al. 2018), our models with $\xi_{\mathrm{env}} = 0.1$ will lose less than 0.2 $\mathrm{M}_\odot$ as failed supernovae only yield large ejecta masses for RSGs where the outer layers contain a considerable amount of mass and are very weakly bound to the star at all. Hence, even at 0.1$Z_\odot$ our evolution model A1 is able to produce a BH of about 80 $\mathrm{M}_\odot$.

6 SUMMARY AND OUTLOOK

In our pilot study, we find BH masses in the range of 80–90 $\mathrm{M}_\odot$ for Z of 10 per cent of the solar value and below. The blue progenitor stars of these BHs retain most of their H envelope due to the inefficiency of line-driven wind mass-loss at these low, but non-extreme metallicities. Low metallicity galaxies of order of 10 per cent the solar value, such as Sextans A, are observed in the Local Universe, and thus there is no need to invoke Population III-type environments for creating heavy BHs. Despite their massive envelope, our model stars never become RSGs, preventing the occurrence of dust-driven mass-loss. We do not consider any binary interactions in our study, but we note that the smaller radial extent of our BSGs limits the interaction frequency with potential companions. For more discussion on binary interactions and Pop III stars, see e.g. Belczynski (2020), Tanikawa et al. (2020), Umeda et al. (2020), and Farrell et al. (2021).

While full grids of stellar evolution models would be necessary to pin down the precise physical limits and exact Z-dependent boundaries between BH formation and PI, we can confidently predict the

maximum BH mass below the PI gap to be of the order of 90–100 $M_\odot$ at low Z (below 10 per cent solar Z). Our predictions on the maximum BH mass are based on evolution models with $M_{\rm init} \sim 90$–$110\,M_\odot$ in the 0.01–0.1 $Z_\odot$ range. At the highest considered metallicity, we find an optimum situation producing an 80 $M_\odot$ BH while avoiding PI, allowing us to constrain the upper stellar mass limit as well as upper Z-limit for *first-generation* BH formation. At larger Z, enhanced wind mass-loss will rapidly drop the maximum BH limit down to the established value of about 50 $M_\odot$. With the occurrence of WR-type mass-loss, which is a strong function of luminosity-to-mass-ratio and Z (Sander et al. 2020; Sander & Vink 2020), the effective BH mass limit can shrink even further (Woosley et al. 2020). As sketched in Fig. 3, the strong mass-loss of massive, envelope-stripped stars during He burning can remove a considerable amount of mass, which further needs to be quantified in dedicated follow-up studies.

Our physically motivated evolution modelling highlights that first-generation BHs can only be ruled out for a small range of masses between approximately 100 and 130 $M_\odot$. The heavy BHs obtained in recent GW events such as GW 190521 show that wind mass-loss at low Z is a crucial ingredient that needs to be carefully considered in stellar evolution and population synthesis modelling to avoid blurring our perception of how the Universe evolved into what we see today. From the analysis and modelling performed here, we may already confidently conclude that for low-Z host galaxies it is possible to create *first-generation* BHs up to values as large as $\sim$ 90 $M_\odot$, without the need to invoke *second-generation* BH formation, extreme assumptions, or exotic physics.

ACKNOWLEDGEMENTS

We warmly thank the MESA developers for making their stellar evolution code publicly available, and the anonymous referee for their detailed and constructive comments. JSV and ERH are supported by STFC funding under grant number ST/R000565/1. AACS is Öpik Research Fellow.

DATA AVAILABILITY

The data underlying this article will be shared on reasonable request to the corresponding author.

REFERENCES

Abbott B. P. et al., 2016, ApJ, 818, L22
Abbott R. et al., 2020, ApJ, 900, L13
Abdul-Masih M. et al., 2020, Nature, 580, E11
Bagnulo S. et al., 2020, A&A, 635, A163
Barkat Z., Rakavy G., Sack N., 1967, Phys. Rev. Lett., 18, 379
Belczynski K., 2020, ApJ, 905, L15
Belczynski K., Bulik T., Fryer C. L., Ruiter A., Valsecchi F., Vink J. S., Hurley J. R., 2010, ApJ, 714, 1217
Belczynski K. et al., 2020, ApJ, 890, 113
Böhm-Vitense E., 1958, Z. Astrophys., 46, 108
Bowman D. M., 2020, Front. Astron. Space Sci., 7, 70
Brott I. et al., 2011, A&A, 530, A115
Burrows A., Radice D., Vartanyan D., Nagakura H., Skinner M. A., Dolence J. C., 2020, MNRAS, 491, 2715
Chatzopoulos E., Wheeler J. C., 2012, ApJ, 748, 42
Chen K.-J., Heger A., Woosley S., Almgren A., Whalen D. J., 2014, ApJ, 792, 44
Choi J., Dotter A., Conroy C., Cantiello M., Paxton B., Johnson B. D., 2016, ApJ, 823, 102
Crowther P. A., Schnurr O., Hirschi R., Yusof N., Parker R. J., Goodwin S. P., Kassim H. A., 2010, MNRAS, 408, 731
de Jager C., Nieuwenhuijzen H., van der Hucht K. A., 1988, A&AS, 72, 259
Ekström S. et al., 2012, A&A, 537, A146
El-Badry K., Quataert E., 2020, MNRAS, 493, L22
Ertl T., Janka H. T., Woosley S. E., Sukhbold T., Ugliano M., 2016, ApJ, 818, 124
Ertl T., Woosley S. E., Sukhbold T., Janka H. T., 2020, ApJ, 890, 51
Farmer R., Renzo M., de Mink S. E., Marchant P., Justham S., 2019, ApJ, 887, 53
Farrell E., Groh J. H., Hirschi R., Murphy L., Kaiser E., Ekström S., Georgy C., Meynet G., 2021, MNRAS, 502, L40
Fernández R., Quataert E., Kashiyama K., Coughlin E. R., 2018, MNRAS, 476, 2366
Fishbach M., Holz D. E., 2020, ApJ, 904, L26
Fowler W. A., Hoyle F., 1964, ApJS, 9, 201
Fragione G., Loeb A., Rasio F. A., 2020, ApJ, 902, L26
Fryer C. L., Woosley S. E., Heger A., 2001, ApJ, 550, 372
Gilkis A., Soker N., Papish O., 2016, ApJ, 826, 178
Glatzel W., Fricke K. J., El Eid M. F., 1985, A&A, 149, 413
Gräfener G., Koesterke L., Hamann W.-R., 2002, A&A, 387, 244
Gräfener G., Owocki S. P., Vink J. S., 2012, A&A, 538, A40
Grassitelli L., Langer N., Mackey J., Graefener G., Grin N., Sander A., Vink J., 2021, A&A, 647, A99
Grevesse N., Sauval A. J., 1998, Space Sci. Rev., 85, 161
Groh J. H., Farrell E. J., Meynet G., Smith N., Murphy L., Allan A. P., Georgy C., Ekstroem S., 2020, ApJ, 900, 98
Heger A., Langer N., Woosley S. E., 2000, ApJ, 528, 368
Higgins E. R., Vink J. S., 2019, A&A, 622, A50
Higgins E. R., Vink J. S., 2020, A&A, 635, A175
Jiang Y.-F., Cantiello M., Bildsten L., Quataert E., Blaes O., Stone J., 2018, Nature, 561, 498
Kalari V. M., Vink J. S., Dufton P. L., Fraser M., 2018, A&A, 618, A17
Kasen D., Woosley S. E., Heger A., 2011, ApJ, 734, 102
Köhler K. et al., 2015, A&A, 573, A71
Kozyreva A. et al., 2017, MNRAS, 464, 2854
Langer N., Norman C. A., de Koter A., Vink J. S., Cantiello M., Yoon S. C., 2007, A&A, 475, L19
Leung S.-C., Nomoto K., Blinnikov S., 2019, ApJ, 887, 72
Liu J. et al. 2019, Nature, 575, 618
Mapelli M., Spera M., Montanari E., Limongi M., Chieffi A., Giacobbo N., Bressan A., Bouffanais Y., 2020, ApJ, 888, 76
Marchant P., Renzo M., Farmer R., Pappas K. M. W., Taam R. E., de Mink S. E., Kalogera V., 2019, ApJ, 882, 36
Moffat J. W., 2020, preprint (arXiv:2009.04360)
Nagataki S., Takahashi R., Mizuta A., Takiwaki T., 2007, ApJ, 659, 512
Nugis T., Lamers H. J. G. L. M., 2000, A&A, 360, 227
O'Connor E., Ott C. D., 2011, ApJ, 730, 70
Orosz J. A., McClintock J. E., Aufdenberg J. P., Remillard R. A., Reid M. J., Narayan R., Gou L., 2011, ApJ, 742, 84
Paxton B., Bildsten L., Dotter A., Herwig F., Lesaffre P., Timmes F., 2011, ApJS, 192, 3
Paxton B. et al., 2013, ApJS, 208, 4
Paxton B. et al., 2015, ApJS, 220, 15
Paxton B. et al., 2018, ApJS, 234, 34
Paxton B. et al., 2019, ApJS, 243, 10
Petit V. et al., 2017, MNRAS, 466, 1052
Petrov B., Vink J. S., Gräfener G., 2016, MNRAS, 458, 1999
Ramírez-Agudelo O. H. et al., 2013, A&A, 560, A29
Renzo M., Cantiello M., Metzger B. D., Jiang Y. F., 2020, ApJ, 904, L13
Rogers F., Nayfonov A., 2002, ApJ, 576, 1064
Romero-Shaw I. M., Lasky P. D., Thrane E., Calderon Bustillo J., 2020, ApJ, 903, L5
Sana H. et al., 2013, A&A, 550, A107
Sander A. A. C., Vink J. S., 2020, MNRAS, 499, 873
Sander A. A. C., Vink J. S., Hamann W. R., 2020, MNRAS, 491, 4406
Scannapieco E., Madau P., Woosley S., Heger A., Ferrara A., 2005, ApJ, 633, 1031
Shaviv N. J., 2000, ApJ, 532, L137

Tanikawa A., Kinugawa T., Yoshida T., Hijikawa K., Umeda H., 2020, preprint (arXiv:2010.07616)
The LIGO Scientific Collaboration & the Virgo Collaboration, 2020, preprint (arXiv:2010.14533)
Tominaga N., 2009, ApJ, 690, 526
Udall R., Jani K., Lange J., O'Shaughnessy R., Clark J., Cadonati L., Shoemaker D., Holley-Bockelmann K., 2020, ApJ, 900, 80
Umeda H., Nomoto K., 2002, ApJ, 565, 385
Umeda H., Yoshida T., Nagele C., Takahashi K., 2020, ApJ, 905, L21
Vink J. S., 2018a, A&A, 615, A119
Vink J. S., 2018b, A&A, 619, A54
Vink J. S., de Koter A., 2005, A&A, 442, 587
Vink J. S., Gräfener G., 2012, ApJ, 751, L34
Vink J. S., de Koter A., Lamers H. J. G. L. M., 2001, A&A, 369, 574
Vink J. S., Brott I., Gräfener G., Langer N., de Koter A., Lennon D. J., 2010, A&A, 512, L7
Vink J. S., Muijres L. E., Anthonisse B., de Koter A., Gräfener G., Langer N., 2011, A&A, 531, A132
Vink J. S. et al., 2015, Highlights Astron., 16, 51
Woosley S. E., 2017, ApJ, 836, 244
Woosley S. E., Heger A., 2012, ApJ, 752, 32
Woosley S. E., Sukhbold T., Janka H. T., 2020, ApJ, 896, 56
Yusof N. et al., 2013, MNRAS, 433, 1114
Zhang W., Woosley S. E., Heger A., 2008, ApJ, 679, 639

This paper has been typeset from a TEX/LATEX file prepared by the author.